Increased ICAM-1 Expression Causes Endothelial Cell Leakiness, Cytoskeletal Reorganization and Junctional Alterations

Paul R. Clark[1,2], Thomas D. Manes[2,3], Jordan S. Pober[1,2,3,4], Martin S. Kluger[1,2]

Tumor necrosis factor (TNF)-induced ICAM-1 in endothelial cells (EC) promotes leukocyte adhesion. Here we report that ICAM-1 also effects EC barrier function. Control- or E-selectin-transduced human dermal microvascular EC (HDMEC) form a barrier to flux of proteins and to passage of current (measured as transendothelial electrical resistance or TEER). HDMEC transduced with ICAM-1 at levels comparable to that induced by TNF show reduced TEER, but do so without overtly changing their cell junctions, cell shape, or cytoskeleton organization. Higher levels of ICAM-1 further reduce TEER, increase F/G-actin ratios, rearrange the actin cytoskeleton to cause cell elongation, and alter junctional zona occludens 1 and vascular endothelial-cadherin staining. Transducing with ICAM-1 lacking an intracellular region also reduces TEER. TNF-induced changes in TEER and shape follow a similar time course as ICAM-1 induction; however, the fall in TEER occurs at lower TNF concentrations. Inhibiting NF-κB activation blocks ICAM-1 induction; TEER reduction, and shape change. Specific small-interfering RNA knockdown of ICAM-1 partially inhibits TNF-induced shape change. We conclude that moderately elevated ICAM-1 expression reduces EC barrier function and that expressing higher levels of ICAM-1 affects cell junctions and the cytoskeleton. Induction of ICAM-1 may contribute to but does not fully account for TNF-induced vascular leak and EC shape change.

Journal of Investigative Dermatology (2007) **127,** 762–774. doi:10.1038/sj.jid.5700670; published online 28 December 2006

INTRODUCTION

Acute inflammation is characterized by a number of changes in local microvessels, including increased leakiness to plasma proteins and increased adhesion of circulating leukocytes to the endothelial cell (EC) lumenal surface (Pober and Cotran, 1991). Plasma protein extravasation is responsible for the classical inflammatory sign of ''tumor'', commonly referred to in skin as edema or induration, and serves to create a provisional matrix within the tissue that can support leukocyte diapedesis. Vascular leakiness may sometimes become more widespread, involving one or more organs, for example in settings of acute respiratory distress syndrome or in systemic sepsis (Crowley, 1996; Groeneveld, 2002). The early changes underlying vascular leakiness have been attributed to concomitant alterations in EC shape and in cell junctions, described as ''retraction'' or ''contraction'', or viewed as inter-endothelial gap formation, respectively (Majno and Palade, 1961; Majno *et al.*, 1969; Wysolmerski and Lagunoff, 1990; McDonald *et al.*, 1999). These morphological changes represent a maximal cytokine response, and protein extravasation may be initiated by more subtle alterations in the endothelial lining.

Leukocyte adhesion involves the transcription and expression of new surface proteins (adhesion molecules) on EC that bind to counter-receptors on circulating leukocytes (von Andrian and Mackay, 2000; Kluger, 2004). Many of these adhesion molecules, including ICAM-1; (CD54) and E-selectin (E-sel) (CD62E), are induced by tumor necrosis factor (TNF; Pober *et al.*, 1986b; Detmar *et al.*, 1990; Richard *et al.*, 1998). Although the regulation of expression of various adhesion molecules differ in detail, all depend upon the transcription factor NF-κB, which is activated by TNF or other proinflammatory cytokines (Collins *et al.*, 1995). Intradermal injection of TNF causes adhesion molecule expression and local extravasation of leukocytes (Munro *et al.*, 1989). TNF is

[1]*Department of Dermatology, Yale University School of Medicine, New Haven, Connecticut, USA;* [2]*Interdepartmental Program in Vascular Biology and Transplantation, Yale University School of Medicine, New Haven, Connecticut, USA;* [3]*Department of Pathology, Yale University School of Medicine, New Haven, Connecticut, USA and* [4]*Department of Immunobiology, Yale University School of Medicine, New Haven, Connecticut, USA*

Correspondence: Dr Martin S. Kluger, 295 Congress Avenue – Room 454, New Haven, Connecticut 06510, USA.
E-mail: martin.kluger@yale.edu

Abbreviations: ANOVA, analysis of variance; EC, endothelial cell; HDMEC, human dermal microvascular EC; SRIκB, mutagenized S32/36A IκBα super repressor of NF-κB; E-sel, E-selectin; ICAM^{basal}, ICAM^{med}, and ICAM^{high}, HDMEC transductants expressing ICAM-1 at basal, medium, or high levels, respectively; ICAM$^{\Delta Cyto}$, HDMEC transductants expressing ICAM-1 with the cytoplasmic domain deleted; PBS, phosphate-buffered saline; siRNA, small-interfering RNA; TEER, transendothelial electrical resistance; TNF, tumor necrosis factor; VE-cadhedrin, vascular endothelial cadhedrin; ZO-1, zona occludens 1

Received 27 February 2006; revised 6 September 2006; accepted 2 October 2006; published online 28 December 2006

also sufficient to produce vascular leak *in vivo*, for example during cytokine-based immunotherapy (Cotran *et al.*, 1988; Lo *et al.*, 1992; Dubinett *et al.*, 1994; Thom *et al.*, 1995). In cell culture, TNF causes EC to undergo cytoskeletal and junctional rearrangements and shape changes (Stolpen *et al.*, 1986; Blum *et al.*, 1997). In particular, actin filaments, concentrated along cell–cell junctions in resting cells, may reorganize as thickened bands or as centrally distributed stress fibers (Stolpen *et al.*, 1986; Wojciak-Stothard *et al.*, 1998). These TNF-induced cytoskeletal changes have been linked to an increase in filamentous (F-) and a simultaneous decrease in globular (G-) actin content (Wojciak-Stothard *et al.*, 1998; Nwariaku *et al.*, 2003). However, the mechanism of such responses to TNF is less well understood than is induction of adhesion molecules. In the present report, we explore the hypothesis that vascular leakiness is mechanistically coupled to adhesion molecule induction, especially of ICAM-1. We propose this concept based on the observations that inflammation-associated leakiness is reduced in ICAM-1$^{-/-}$ mice (Sligh *et al.*, 1993; Xu *et al.*, 1994) and that the intracellular cytoplasmic tail of ICAM-1 interacts directly with actin-binding proteins, such as actinin, ezrin, and moesin (Carpen *et al.*, 1992; Heiska *et al.*, 1998; Barreiro *et al.*, 2002). In addition, when crosslinked by antibody or engaged by leukocytes, ICAM-1 can reorganize the actin cytoskeleton (Amos *et al.*, 2001; Wang *et al.*, 2002) by acting through a Rho-dependent pathway (Adamson *et al.*, 1999). Here we show that simple overexpression of ICAM-1 in cultured human dermal microvascular EC (HDMEC) can cause vascular leakiness as well as EC shape change, cytoskeletal reorganization, and junctional protein alterations in the absence of crosslinking or leukocyte binding. Like ICAM-1 induction, TNF-induced leakiness and shape change require NF-κB-induced protein synthesis. However, our studies using siRNA suggest that even though increased expression of ICAM-1 contributes to TNF-initiated responses, it does not wholly account for them.

RESULTS

Effects of ICAM-1 overexpression

Cultured HDMEC grown to confluence on fibronectin-coated transwell inserts form a monolayer that resists the passage of electrical current, which may be quantified as a transendothelial electrical resistance (TEER). To examine the effects of ICAM-1 expression on barrier function, we produced a series of retrovirally transduced HDMEC cell lines. These consisted of cell lines that expressed ICAM-1, E-sel, or control transductants (made with empty viral vector). By FACS analysis, control transductants expressed ICAM-1 at levels comparable to basal expression on non-transduced HDMEC, and are therefore designated as ICAM-1^{basal}. Cell lines that expressed ICAM-1 at levels comparable to that seen following TNF are designated as ICAM-1^{med} and cell lines that expressed approximately 8-fold higher levels are designated as ICAM-1^{high}. Neither ICAM-1^{basal}, ICAM-1^{med}, nor ICAM-1^{high} expressed E-sel. E-sel transductants E-sel expressed E-sel at levels comparable to that observed in TNF-treated HDMEC, but remained at basal levels for ICAM-1 (Figure 1a). We plated E-sel, ICAM-1^{basal}, and ICAM-1^{med} on fibronectin-coated transwells and measured TEER on a daily basis as the cells reached confluence. TEER increased daily, reaching a plateau of maximal TEER 48–72 hours post-visual confluence. The level of TEER achieved by ICAM-1^{med} monolayers was significantly lower than that achieved by ICAM-1^{basal} or E-sel (shown in Figure 1b, upper panel). ICAM-1^{high} monolayers established very little TEER, approaching that of naked transwells (Figure 1b, lower panel). The effects of different levels of transduced ICAM-1 expression on TEER were reproducible in three separately derived sets of transductants, analyzed in multiple independent experiments.

To determine if the fall in monolayer TEER observed with increasing ICAM-1 expression by HDMEC represents a change in macromolecular permeability, we cultured ICAM-1^{basal}, ICAM-1^{med}, and ICAM-1^{high} HDMEC transductants on transwells until TEER became maximal and measured the transmonolayer flux of FITC-tagged BSA. The flux of FITC-BSA across naked transwells was much greater than across transwells containing post-confluent HDMEC, indicating that HDMEC formed a monolayer with barrier function toward BSA (data not shown). The passage of FITC-BSA accelerated with increasing levels of HDMEC ICAM-1 expression (Figure 1c), and as reported by others (Marcus and Gewertz, 1998) the rate of protein flux was inversely proportional to TEER. These differences in transmonolayer flux of BSA and in TEER cannot be ascribed to reduced cell density, as ICAM-1^{med} and ICAM^{high} cells reached equivalent if not greater numbers at 48 hours post-confluence than did ICAM-1^{basal} or E-sel (data not shown).

The creation of an endothelial barrier has been correlated with the organization of actin filaments into dense peripheral bands; vascular leakiness occurs at sites where actin filaments rearrange into longitudinal stress fibers (Stolpen *et al.*, 1986; Brett *et al.*, 1989). This reorganization of actin filaments also results in a change in cell shape from polygonal to elongated (Wojciak-Stothard *et al.*, 1998). These observations have been used to infer that a reorganization of the actin cytoskeleton underlies the development of leakiness. To examine this hypothesis, we quantified cell shape in confluent monolayers of our transductants by determining ratios of the longest to the shorter perpendicular axis of HDMEC (an ''axis ratio'') from morphometrical measurements, using the staining pattern of the junctional protein vascular endothelial (VE)-cadherin as a guide. The majority of ICAM-1^{high} cells were elongated in cell shape relative to ICAM-1^{basal} controls or E-sel HDMEC (quantified morphometrically in Table 1). This difference in ICAM-1^{high} shape could also be visualized by phalloidin staining as a thickening of the actin stress fibers (Figure 2a). Importantly, despite lower TEER relative to ICAM^{basal}, visible elongation and reorganization of actin filaments were not observed for ICAM^{med}.

As TNF-induced leakiness has been correlated with an increase in the filamentous (F-) to monomeric (G-) actin ratio (Wojciak-Stothard *et al.*, 1998), we examined whether this ratio may be directly affected by ICAM-1. Compared to E-sel,

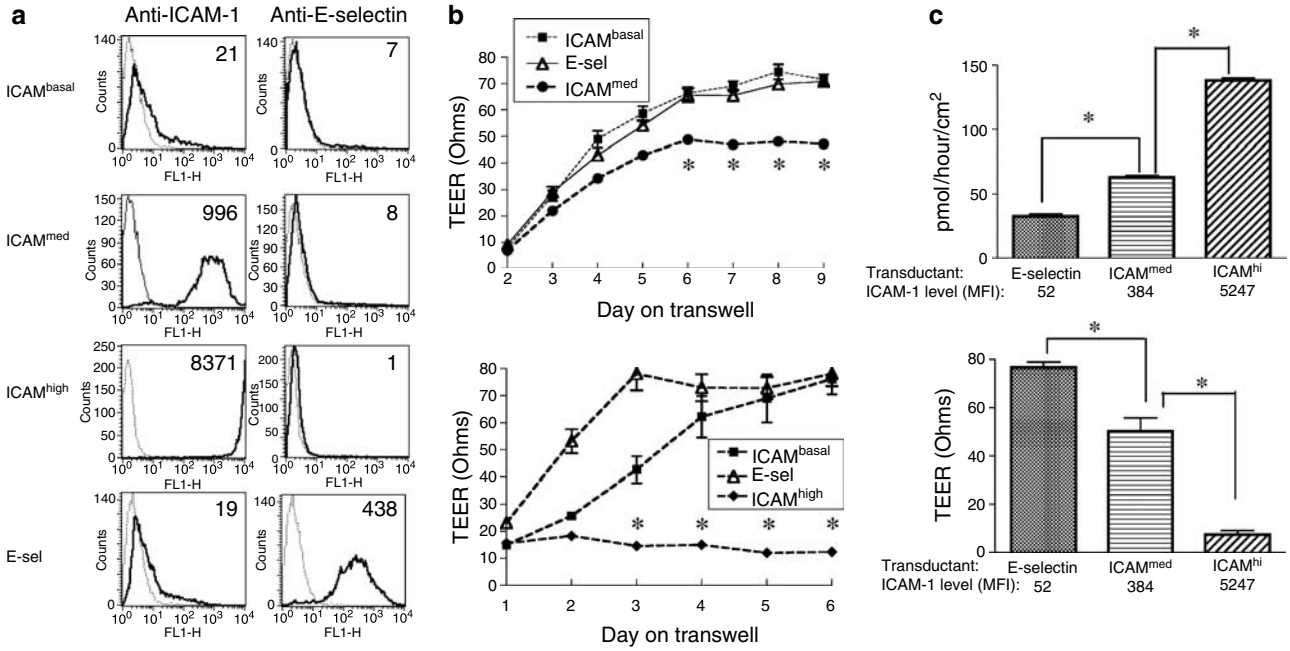

Figure 1. Adhesion molecule expression and permeability measurements on HDMEC transductants. (**a**) Adhesion molecule expression as assessed by direct immunofluorescence and FACS analysis is presented in histograms plotting fluorescence intensity (logarithmic *x* axis) versus cell number (*y* axis). Immunostaining with anti-ICAM-1 and anti-E-sel (dark lines), isotype-matched control (light lines) and the mean fluorescence intensity (MFI) corrected for isotype control are shown. (**b**) TEER properties of HDMEC transductants. TEER measurements on ICAM^{med} (top) and ICAM^{high} (bottom) HDMEC transductants were recorded daily and compared to those on ICAM^{basal} (empty vector control transduced) and E-sel HDMEC. TEER levels (*y* axis) are the mean electrical resistance in ohms ± SEM corrected for the resistance of a naked transwell. *$P<0.001$ by two-way ANOVA, Bonferroni post-test ($n=6, 6, 6$). Shown are two out of a total of five independent experiments involving three separately derived HDMEC lines for each construct. (**c**) Comparison of TEER with flux of BSA across transwells of transduced HDMEC monolayers. By FACS analysis HDMEC expressed ICAM-1 at basal, medium, or high levels. After measuring TEER, FITC-tagged BSA was added to the upper chamber of each transwell. The molar amount of BSA collected from the bottom chamber was used to determine a flux rate based on the transwell surface area (0.3 cm^2) and the duration of the flux assay (20 hours). *$P<0.001$ by one-way ANOVA, Bonferroni post-test ($n=6, 6, 6$). Representative of two independent experiments.

Table 1. Cell shape comparison among HDMEC transductants

Construct	Axis ratio
ICAM^{basal}	3.2 ± 0.21
ICAM^{med}	2.7 ± 0.17
ICAM^{high}	4.5 ± 0.32*
E-sel	3.1 ± 0.21

E-sel, E-selectin; HDMEC, human dermal microvascular endothelial cell. Morphometry units are the mean ratio of the longest axis and perpendicular short axis ± SEM measured on individual HDMEC immunostained for VE-cadherin. *$P<0.01$ by one-way ANOVA, Dunnett's post-test. Representative of three independent experiments with transduced HDMEC derived from two different skin sources, $n=50$ per group.

the F/G actin ratio is increased nearly 3-fold in ICAM^{high} transductants by immunoblot analysis of lysates obtained by differential detergent extraction (Figure 2b). However, no increase in the F/G actin ratio of ICAM^{med} was observed relative to that of E-sel or ICAM^{basal} (in two independent experiments with two different HDMEC lines; data not shown). These results suggest that re-organization of the actin cytoskeleton underlies shape changes we observed at higher levels of ICAM-1 expression. However, higher levels of ICAM-1 are required to reorganize the actin cytoskeleton than are required to reduce TEER.

Two different types of intercellular junctions composed of different molecular structures normally maintain permselectivity of EC to blood macromolecules, namely tight junctions, formed by occludin, claudins, junctional adhesion molecules and associated zona occludens 1 (ZO-1), and adherens junctions, formed by VE-cadherin and catenins (Stevens *et al.*, 2000; Bazzoni and Dejana, 2004). As TNF treatment disrupts the otherwise continuous staining patterns of junctional molecules like ZO-1 (at tight junctions, Blum *et al.*, 1997) and VE-cadherin (at adherens junctions; Wojciak-Stothard *et al.*, 1998; Corada *et al.*, 1999) we examined whether the distribution patterns of these proteins might be affected by increased ICAM-1. The immunostaining patterns for VE-cadherin and ZO-1 were disjoined and fainter in ICAM^{high} compared to E-sel and ICAM^{med} transductants, which more closely resembled ICAM^{basal} (non-transduced) control HDMEC (Figure 3). Compared with other HDMEC transductants, VE-cadherin, and ZO-1 immunostaining patterns of ICAM^{high} appeared visibly fragmented and interdigitized along the paracellular boundaries. We quantified

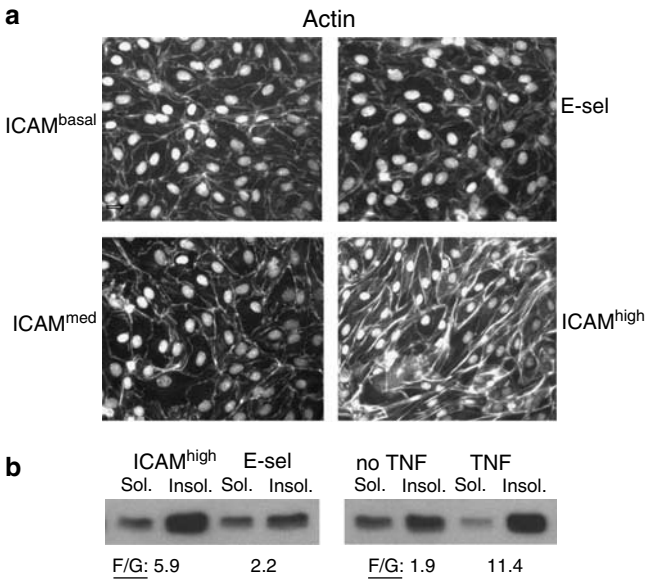

Figure 2. Cytoskeletal re-organization among HDMEC transductants. (**a**) Changes in actin cytoskeleton organization among HDMEC transductants were visually assessed by phalloidin staining of filaments and 4′,6-diamidino-2-phenylindole, dihydrochloride staining of nuclei. The actin cytoskeleton organization of ICAM^{basal}, ICAM^{high}, ICAM^{med}, and E-sel HDMEC are shown. Bar = 10 μm. Representative of three independent experiments using two separately derived HDMEC lines. (**b**) Immunoblot analysis of cytoskeleton re-organization. The bands shown represent the relative amounts of F- and monomeric G- forms of β-actin, derived from detergent insoluble (insol.) and detergent soluble (sol.) protein lysates, respectively (see Materials and Methods), obtained from ICAM-1 and E-sel transductants (left) and non-transduced HDMEC either treated with vehicle or TNF (10 ng/ml for 24 hours; right). The F-/G-actin ratio shown below was determined by densitometry for each HDMEC condition after detection with mouse anti-β-actin mAb. Representative of three or more independent experiments with three different lines of transduced HDMEC and four different lines of non-transduced HDMEC.

patterns of immunostained junctions using morphometry software (Image J) according to a method established by others (Macconi *et al.*, 2006). For two different lines of ICAM^{high}, the number of tight junction-associated ZO-1 segments increased and the length per segment decreased compared to E-sel control HDMEC (Tables 2 and 3). Again compared with E-sel, in ICAM^{med} the number of ZO-1 segments increased and length per segment decreased, but to a lesser extent than for ICAM^{high} (Table 2). However, this comparison did not reach statistical significance in the

Table 2. Morphometric analysis of ZO-1 and VE-cadherin immunostaining at HDMEC junctions

Antibody	Transductant	Segments/field	Mean segment length/field (in μm)
Anti-ZO-1	ICAM^{med}	402.2 ± 22.4*	2.96 ± 0.13**
	ICAM^{high}	788.8 ± 60.3*	1.77 ± 0.06*
	E-sel (control)	264.4 ± 22.2	4.31 ± 0.33
Anti-VE-cadherin	ICAM^{med}	657.8 ± 24.9*	2.06 ± 0.06
	E-sel (control)	583.9 ± 24.0	2.04 ± 0.09

E-sel, E-selectin; HDMEC, human dermal microvascular endothelial cell; VE, vascular endothelial; ZO-1, zona occludens 1.
For these HDMEC lines derived from the same skin donor, morphometric analysis of tight junction ZO-1, and adherens junction VE-cadherin immunostaining was performed after fixing in ethanol/acetic acid (for detection of intracellular ZO-1) or in paraformaldehyde (for detection of transmembrane VE-cadherin).
Statistical significance was determined with reference to E-sel control transductants.
*P<0.05, **P<0.01 by one-way ANOVA, Dunnett's post-test. *P<0.05 by unpaired t-test.

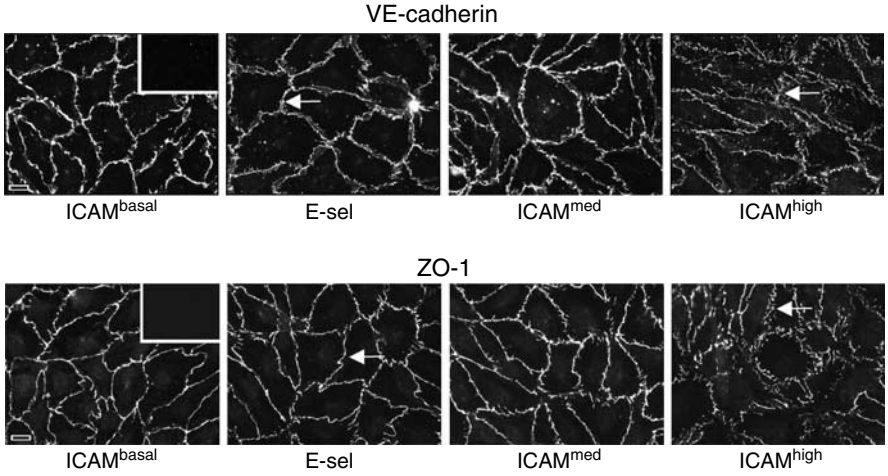

Figure 3. Assessment of changes in adherens and tight junctions among HDMEC transductants. The adherens junctions and tight junctions of HDMEC transductants fixed in ethanol/5% acetic acid were visualized by immunostaining with goat anti-VE-cadherin and mouse anti-ZO-1, respectively. Fragmented and interdigitized junctional immunostaining of VE-cadherin and ZO-1 in ICAM^{high} differed from that of E-sel (arrows) which appeared continuous, more like that of non-transduced ICAM^{basal} control HDMEC. Antibody specificity was assessed by pre-adsorbing anti-VE-cadherin with immunogenic peptide before immunostaining (top left inset) and by comparing anti-ZO-1 with a mouse IgG_1 isotype control (bottom left inset). Bar = 10 μm.

Table 3. Morphometric analysis of ZO-1 and VE-cadherin immunostaining at HDMEC junctions

Antibody	Transductant	Segments/field	Mean segment length/field (in μm)
Anti-ZO-1	ICAM^{med}	561±38.4	2.21±0.093
	ICAM^{high}	830±25.3*	1.42±0.047*
	E-sel (control)	488±26.5	2.22±0.14
Anti-VE-cadherin	ICAM^{med}	943±105.0	1.54±0.100
	ICAM^{high}	1496±56.5*	1.40±0.057
	E-sel (control)	986±96.9	1.47±0.087

E-sel, E-selectin; HDMEC, human dermal microvascular endothelial cell; VE, vascular endothelial; ZO-1, zona occludens 1.
Morphometric analysis of ZO-1 and VE-cadherin immunostaining in transduced HDMEC lines derived from a second, different donor than in Table 2.
The ZO-1 segment length/field measurement for ICAM^{med} but not for E-sel was statistically greater that of non-transduced control HDMEC ($P<0.05$; data not shown).
Both tight junction ZO-1 and adherens junction VE-cadherin immunostaining was performed after fixing in ethanol/acetic acid.
Statistical significance was determined with reference to E-sel control transductants.
*$P<0.001$ by one-way ANOVA, Dunnett's post-test.

Table 4. Morphometric analysis of shape change of SRIκB-transduced HDMEC

HDMEC line	TNF treatment	Cell shape ratio
Vector-transduced	–	1.8±0.1
Vector-transduced	+	3.7±0.3*
SRIκB	–	2.1±0.1
SRIκB	+	1.9±0.1

HDMEC, human dermal microvascular endothelial cell; SRIκB, mutagenized S32/36A IκBα super repressor of NF-κB.
Assessment of TNF-induced shape change in SRIκB-transduced HDMEC compared to vector-transduced HDMEC. Morphometry units are the mean ratio of the longest axis and perpendicular short axis±SEM measured on individual HDMEC immunostained for VE-cadherin.
Representative of four independent experiments using HDMEC derived from two different skin sources, n=50 per group.
*$P<0.01$ versus untreated vector-transduced HDMEC by one-way ANOVA, Dunnett's post-test.

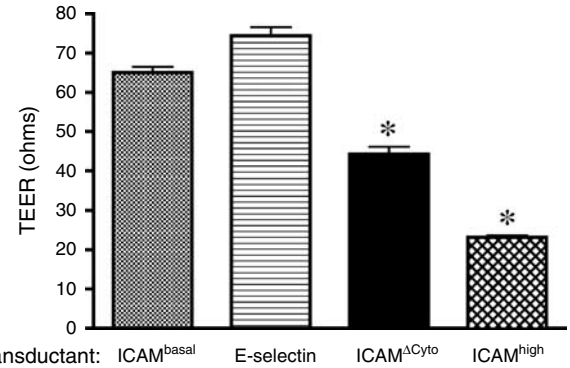

Figure 4. TEER properties of ICAM$^{\Delta Cyto}$ HDMEC. TEER measurements were recorded daily on ICAM$^{\Delta Cyto}$ HDMEC and compared to those on vector-transduced ICAM-1^{basal}, E-sel, and ICAM^{high} HDMEC. TEER levels (y axis) are the mean electrical resistance in ohms±SEM corrected for the resistance of a naked transwell. *$P<0.01$ versus ICAM^{basal} by two-way ANOVA, Bonferroni post-test, $n=5$ per transductant. Representative of a total of six independent experiments involving two differently derived HDMEC ICAM$^{\Delta Cyto}$ transductants.

second of two ICAM^{med} lines examined (Table 3). E-sel measurements were comparable to those of non-transduced HDMEC by this analysis (data not shown). Extensive redistribution of VE-cadherin surface expression away from intercellular adherens junctions was observed in paraformaldehyde-fixed ICAM^{high} that prevented evaluation by this method (data not shown). In ethanol- and acetic acid-fixed ICAM^{high}, however, intracellular, presumably cytoskeleton-associated VE-cadherin could be evaluated and by this approach the number of adherens junction-associated VE-cadherin segments was increased and the segment length decreased compared to E-sel control HDMEC (Table 3). For ICAM^{med}, the number of adherens junction-associated VE-cadherin segments increased in one of the two lines examined, but there were no differences measured in segment length (Tables 2 and 3). These measurements support visually apparent differences in ICAM^{high} ZO-1 and VE-cadherin immunostaining and suggest that more subtle junctional differences among ICAM^{med} and E-sel control are detectable, but vary among the two lines of transductants examined.

Our initial hypothesis was that because ICAM-1 interacts with the actin cytoskeleton through its intracellular region, increased levels of ICAM-1 expression would perturb the actin cytoskeleton, affecting cell junctions, and paracellular permeability. However, the experiments described above suggest that effects on permeability may be uncoupled from effects on the cytoskeleton requiring higher levels of ICAM-1 expression. To explore this idea further we generated a truncated form of ICAM-1 that lacked all but one residue of the ICAM-1 cytoplasmic domain (ICAM$^{\Delta Cyto}$) and should thus be incapable of directly interacting with the actin cytoskeleton. As only a portion of HDMEC expressed ICAM$^{\Delta Cyto}$ above basal levels following our standard transduction procedure, we isolated this population by FACSort (Figure S1). In two different lines of transduced HDMEC, TEER was lower in FACSorted ICAM$^{\Delta Cyto}$ than in ICAM^{basal} and E-sel, but in each case not as low as in ICAM^{high} (Figure 4). These results suggest that regions outside of the ICAM-1 cytoplasmic domain can contribute to vascular leakiness.

Effects of TNF-treatment on ICAM-1 expression, leakiness, and shape change

As overexpressing ICAM-1 in HDMEC was observed to cause changes in TEER and cytoskeletal organization resembling those caused by TNF, we assessed the potential contributions

of ICAM-1 to TNF-induced leakiness by comparing the quantitative and kinetic relationships of TNF-induced ICAM-1 expression to TNF-induced changes in TEER and shape. We first added 10 ng/ml TNF to a confluent HDMEC monolayer and followed the effect on ICAM-1 expression over time. TNF-treated HDMEC showed no change in their basal expression level of ICAM-1 for at least 1 hour, markedly increased their expression level at 4 hours and even further increased their expression level at 24 hours (Figure 5a). In replicate TNF-treated HDMEC cultures we observed that the time dependence of the TEER response was similar to that observed for induction of ICAM-1 expression; TEER was sustained for at least 1 hour before decreasing at 4 hours, and falling even further by 24 hours, compared to a vehicle-treated monolayer (Figure 5b). The time dependence of the TNF-induced HDMEC elongation response was somewhat slower than those of ICAM-1 expression or TEER, not changing during the first 4 hours but visually apparent at 24 hours (Figure 5c). TNF-treated HDMEC that had undergone shape change also showed a 6-fold increase in actin polymerization (Figure 2b). We then compared the HDMEC response of TNF to that of thrombin, an agent known to cause rapid increases in vascular permeability. In contrast to the TNF response, thrombin caused a fall of TEER within 10 minutes that returned to baseline by 24 hours (Figure 5b). Moreover, unlike TNF, thrombin did not increase expression of ICAM-1 or change HDMEC shape, further emphasizing that differing mechanisms underlie the actions of these two inflammatory mediators (data not shown).

We next examined the concentration dependence of these three responses at 48 hours of TNF treatment. Pilot experiments established that all three TNF-induced changes were maximal at 10 ng/ml. A 50% maximal change in ICAM-1 expression and in cell elongation each occurred at 1.1 ng/ml TNF. In contrast, only 0.13 ng/ml was required to produce a 50% of maximum fall in TEER (Figure 5d–f). Collectively, these data suggest that while increased ICAM-1 expression may contribute to TNF-induced leakiness, it does not wholly account for it.

Contributions of increased ICAM-1 expression to TNF-induced leakiness and shape change

To more directly assess the contributions of ICAM-1 to TNF-induced leakiness and EC shape change, we pursued two parallel strategies. First, we blocked ICAM-1 induction by interference with TNF-induced gene transcription. Many TNF-induced transcriptional events in EC, including that of ICAM-1, are controlled by NF-κB activation, which is repressed by IκBα in the absence of TNF (Collins *et al.*, 1995). TNF-mediated NF-κB activation can be blocked by

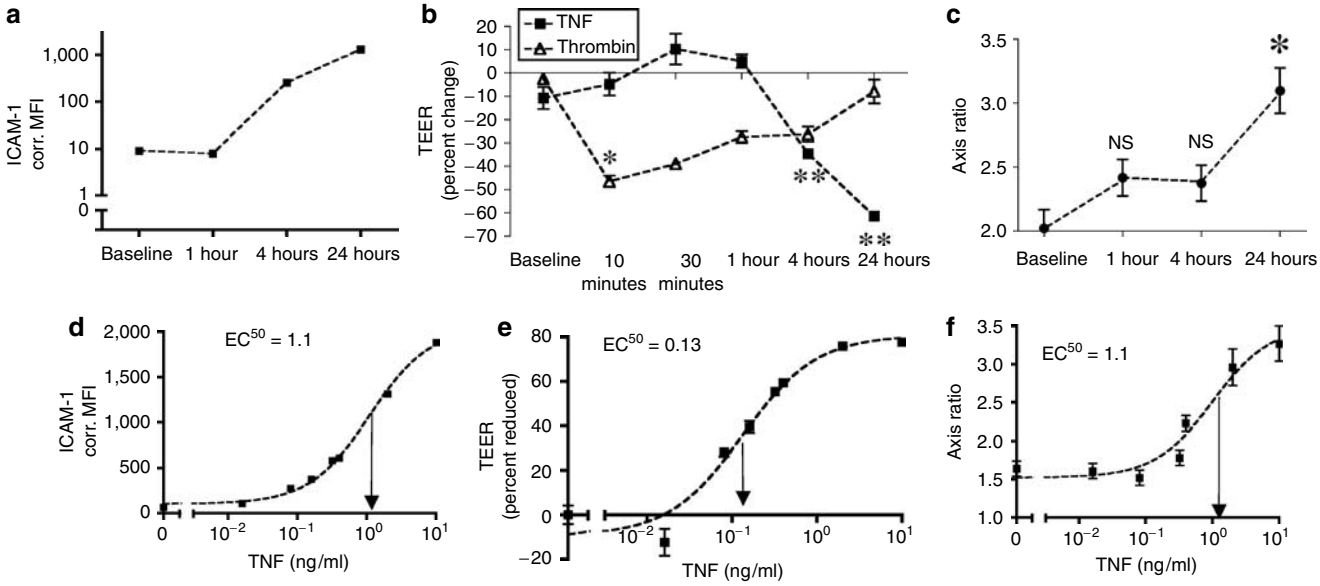

Figure 5. HDMEC responses to TNF. (**a–c**) Time dependence of HDMEC TNF responses. (**a**) FACS analysis of ICAM-1 expression through 24 hours of TNF quantified as the isotype-corrected MFI of anti-ICAM-1-FITC immunostaining (logarithmic *y* axis). (**b**) TEER measurements of TNF-induced leakiness. TEER was reduced at 4 hours of TNF (10 ng/ml) versus at 10 minutes of thrombin (2 NIH U/ml). The cytokine-induced fall in TEER is expressed as the percentage different from TEER of vehicle-treated control HDMEC (percent change, *y* axis; described in Materials and Methods).**$P<0.001$ for TNF ($n=6$) versus control ($n=5$), *$P<0.001$ for Thrombin ($n=6$) versus control by two-way ANOVA, Bonferroni post-test. Representative of three independent experiments with similar results. (**c**) Quantitative morphometry of TNF-induced shape change. TNF-induced shape change was delayed, first detected after 4 hours of TNF treatment. Replicate monolayers of untreated HDMEC showed no change in shape over the same period (data not shown). *$P<0.01$ versus baseline (pre-TNF treatment); NS, not significant by one-way ANOVA, Bonferroni post-test. Representative of three independent experiments. (**d–f**) Concentration dependence of TNF responses. (**d**) By FACS analysis, ICAM-1 expression increased as a function of TNF concentration, reaching 50% of the measured change at 1.1 ng/ml TNF. (**e**) TEER was reduced by 50% at 0.13 ng/ml TNF, an approximately 10-fold less concentration than that required for a 50% increase in ICAM-1 expression or cell shape. The TNF-induced fall in TEER was calculated relative to the TEER of vehicle-treated HDMEC as in Figure 5b, except is expressed as a positive value for comparison with the HDMEC ICAM-1 and shape responses to TNF (percent reduction, *y* axis) (**f**) By morphometry, HDMEC shape elongated 50% at a TNF concentration of 1.1 ng/ml. Data in (**d–f**) are representative of two independent experiments with HDMEC obtained from different skin sources.

overexpression of a mutagenized S32/36A IκBα that acts as a ''super repressor'', designated SRIκB. Compared to enhanced green fluorescent protein transductants, SRIκB-HDMEC showed reduced nuclear translocation of Rel A (also known as the p65 subunit of NF-κB) in response to TNF (data not shown) and reduced (but did not eliminate) basal and inducible expression of ICAM-1 (Figure S2). Strikingly, SRIκB-transduced HDMEC did not lose TEER in response to TNF (through 48 hours) despite retaining a rapid TEER loss in response to thrombin (Figure 6). TNF also failed to induce shape change in SRIκB-transduced HDMEC derived from two different skin sources (quantified in Table 4) an inhibition that was clearly visible at the level of the actin cytoskeleton (data not shown). These data show that TNF-induced TEER loss and shape change require NF-κB inducible protein expression in HDMEC, but they do not directly link ICAM-1 to this process.

Our second strategy to connect ICAM-1 to TNF-mediated responses involved the use of siRNA to specifically reduce ICAM-1 expression. We analyzed four different siRNA sequences specific to ICAM-1 and compared our results to an irrelevant siRNA (nuclear lamin A; siRNA sequences are listed in Table S1). Unfortunately, the oligofectamine-based transfection procedure itself caused a significant fall in TEER making it impossible to unambiguously assign effects to specific siRNA molecules with this assay. However, transfection did not alter cell shape. In this case, three different siRNA sequences that reduced ICAM-1 expression (without affecting E-sel; data not shown) did reduce the extent of cell elongation caused by TNF (Table 5). However, the magnitude of the effects on ICAM-1 expression and cell elongation did not strictly correlate. This was evident with siRNA 731 which could reduce the level of ICAM-1 surface expression without blocking shape change. These data support a role for ICAM-1 in mediating the TNF effects on the HDMEC cytoskeleton, but indicate that other proteins requiring NF-κB activation for their TNF-inducible expression are also involved in this response.

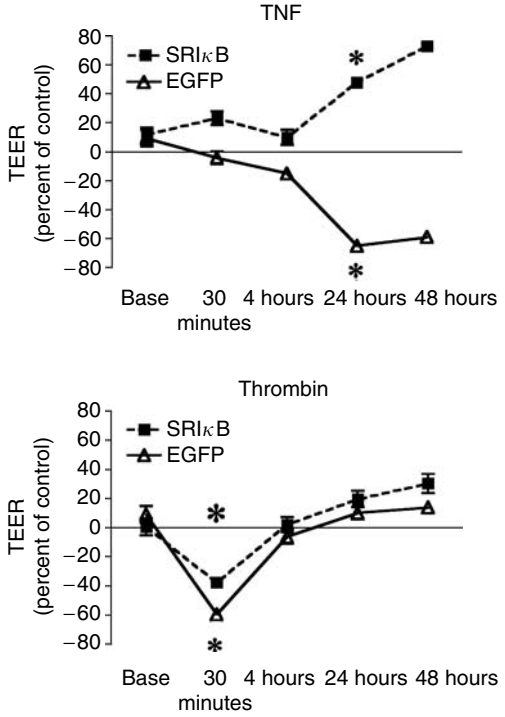

Figure 6. Responses of SRIκB- and enhanced green fluorescent protein-transduced HDMEC to TNF. TNF-induced leakiness is blocked in SRIκB HDMEC. Leakiness in response to either 10 ng/ml TNF (top) or 2 NIH U/ml thrombin (bottom) is expressed as a percent of TEER measured on vehicle-treated replicate cultures (*y* axis) **P*<0.01 by two-way ANOVA, Bonferroni post-test. Representative of three independent experiments and HDMEC obtained from two different skin sources.

DISCUSSION

We hypothesized that induction of ICAM-1 can cause leakiness in HDMEC monolayers and present data showing that retrovirally transduced ICAM-1 causes reduced TEER and overt alterations to the actin cytoskeleton and endothelial junctions. Compared to ICAM^{basal} control and E-sel, leak was increased at TNF-inducible levels of ICAM-1 expression (ICAM^{med}), measured as a significant (>25%) fall in TEER and a doubling of the transmonolayer flux rate of FITC-BSA (Figure 1). At high levels of ICAM-1 expression, thickening of the actin stress fibers was visibly apparent (Figure 2). Moreover, this change was correlated with a transition from the detergent soluble to the detergent insoluble fraction that we measured as an increased F/G actin ratio. High levels of ICAM-1 expression also produced quantifiable gaps in ZO-1 and VE-cadherin immunostaining (Figure 3 and Tables 3 and 4). Finally, we show that the effects of ICAM-1 overexpression on TEER and the actin cytoskeleton reside, at least in part, outside of the ICAM-1 cytoplasmic tail (Figure 4).

The ability of ICAM$^{\Delta Cyto}$ to reduce TEER was unexpected. Such effects are presumably mediated by interactions of the extracellular and/or transmembrane regions of ICAM-1 with other membrane proteins. Possible interactive targets include junctional proteins and/or other transmembrane proteins (including full-length endogenous ICAM-1) that couple to the cytoskeleton. The effect of ICAM$^{\Delta Cyto}$ on actin reorganization was variable (data not shown). Although we did not directly compare ICAM$^{\Delta Cyto}$ expression among different transductants, our data would suggest that such differences (like those of ICAM^{med} on endothelial junctions) may derive from differences in the level of ICAM-1 expressed. We have been unable to assess the effect of overexpressing the ICAM-1 cytoplasmic domain directly. A chimeric construct consisting of the ICAM-1 cytoplasmic domain linked to the extracellular and transmembrane domains of E-sel, showed TEER equivalent to that of ICAM^{basal}, but because expression levels were consistently and considerably less than that of ICAM^{med}, it was not possible to definitively assess the role of the ICAM-1 cytoplasmic domain. Experiments using dominant-negative peptides based on the ICAM-1 cytoplasmic domain have been inconsistent (unpublished observations, MSK).

An important message of these studies is that leakiness does not appear to require major cytoskeleton-based changes in cell shape or major alterations in junctional protein

Table 5. Effect of siRNA knockdown on EC shape

Experiment	Condition	ICAM-1 expression (MFI corrected for isotype control)	Cell shape (axis ratio)	Percentage siRNA knockdown of TNF-induced ICAM-1 expression[1]	Percentage siRNA-dependent inhibition of TNF-induced shape change[2]	Two-tailed unpaired *t*-test for shape change after TNF versus TNF+siRNA
One	No TNF	32	1.8	—	—	—
	TNF	1,308	3.3	—	—	—
	TNF+741	233	2.1	84.2	80.0	$P<0.0001$
Two	No TNF	46	1.8	—	—	—
	TNF	1,685	3.1	—	—	—
	TNF+741	358	2.3	81.0	61.5	$P<0.003$
	TNF+lamin	1,903	3.3	−13.3	−15.4	NS
Three	No TNF	19	1.8	—	—	—
	TNF	1,502	2.5	—	—	—
	TNF+756	302	1.9	80.9	85.7	$P<0.03$
	TNF+749	471	1.7	69.5	114.3	$P<0.005$
	TNF+731	600	2.5	60.8	0.0	NS
	TNF+lamin	1,728	2.5	−15.2	0.0	NS

EC, endothelial cell; NS, not significant; siRNA, small-interfering RNA; TNF, tumor necrosis factor.
[1]The siRNA knockdown of TNF-induced ICAM-1 expression is expressed as a percentage of TNF-induced ICAM-1 expression: $[((\text{corrected MFI}^{TNF} - \text{corrected MFI}^{No\ TNF}) - (\text{corrected MFI}^{TNF+siRNA} - \text{corrected MFI}^{No\ TNF}))/(\text{corrected MFI}^{TNF} - \text{corrected MFI}^{No\ TNF})] \times 100$.
[2]The siRNA-dependent inhibition of TNF-induced shape change is expressed as a percentage of TNF-induced shape change: $[((\text{EC shape}^{TNF} - \text{EC shape}^{No\ TNF}) - (\text{EC shape}^{TNF+siRNA} - \text{EC shape}^{No\ TNF}))/(\text{EC shape}^{TNF} - \text{EC shape}^{No\ TNF})] \times 100$.

organization. This conclusion is based upon differences in ICAM-1 (and TNF) levels needed to change these parameters (Table 1 and Figures 2a, 5e and f), and upon different time courses of TNF needed for their occurrence (Figure 5b and c). And based on examination and analysis of cell–cell junctions, leakiness does not appear to require major alterations to junctional protein organization (Figure 3; Tables 2 and 3). The observed differences suggest either that barrier function can be regulated independently from the cytoskeleton, or that a greater signal strength, operating through the same mechanism, is necessary for evoking shape change than vascular leak. In other words, our data do not rule out the possibility that the actin cytoskeleton could be a common mediator of both responses, potentially altering junctional proteins in a manner not detectable by the assays used in this study.

Having established that ICAM-1 expression can cause vascular leak, we then investigated whether increased expression of ICAM-1 contributes to the development of vascular leak in response to the proinflammatory cytokine TNF. Our most direct observations in support of this concept are that HDMEC expressing levels of ICAM-1, but not of E-sel, comparable to those induced by TNF show both a loss of TEER and an increase in the passage of BSA proportional to their level of ICAM-1 expression. Transduction of ICAM-1 also produced visible changes in the actin cytoskeleton, measured as an elongation in cell shape, and an increased F/G actin ratio, that were quantitatively similar to those seen in TNF-treated cells. The contribution of ICAM-1 to the effects of TNF on TEER was further supported by the ability of SRIκB, a super repressor of NF-κB activation, to block both TNF induction of ICAM-1 expression and TNF reduction of TEER. However, ICAM-1 is likely to account only partially for the effect of TNF on TEER, because TEER was reduced at lower TNF concentrations than were needed to induce ICAM-1 expression. TNF-induced shape change also was reduced by specific siRNA knockdown of ICAM-1 expression. However, once again, this activity of ICAM-1 is likely to account only partially for the effect of TNF, as an equivalent shape change required higher levels of ICAM-1 in transductants than in TNF-treated HDMEC, and because the effects of siRNA knockdown of ICAM-1 expression were not fully concordant with effects on cell shape. Our approaches taken to reduce ICAM-1 expression or effects have limitations. Our SRIκB HDMEC are fully refractory to TNF-induced permeability, consistent with a contributory role for ICAM-1 in TNF-induced leak, but this approach inhibited TNF-induced synthesis of many proteins in addition to ICAM-1. SiRNA experiments, which are more specific to ICAM-1, may be complicated by unpredictable off-target effects (the siRNA

oligomer that knocked down ICAM-1 without affecting shape change may have induced a compensatory off target effect that went undetected). We addressed this by using four different sequences that were screened to rule out strong induction of interferon-related genes. Despite these limitations, the similar outcome from these different approaches strengthens our primary conclusion, namely that increasing ICAM-1 expression induces vascular leak and shape change. Additionally, these data suggest that in the context of EC activation by TNF treatment, increased ICAM-1 expression may contribute to the effects of TNF on vascular leak through cytoskeletal re-organization.

It is clear from our studies that changes in TEER and HDMEC shape following TNF require new, NF-κB-dependent protein synthesis. In this regard our data differ from a recent study in which reduction of TEER by TNF required ezrin/radixin/moesin phosphorylation, detected before induction of ICAM-1 expression by TNF (Koss *et al.*, 2006). Our data also differ from another study that reported rapid, rho-dependent responses to TNF in HUVEC (Wojciak-Stothard *et al.*, 1999). Factors that may explain these differences are that we used a different EC type, namely HDMEC, that form an effective barrier to passage of electrical current, and that our transwell measurements were not performed until maximal levels of TEER were reached at 48–96 hours post-confluence. It will be important to investigate whether or not changes in EC permeability owing to ICAM-1 occur independently from changes owing to TNF-induced ezrin/radixin/moesin phosphorylation or Rho activation. Our data suggest that the mechanism and speed of these TNF effects differ from that of thrombin, a trimeric G-protein coupled receptor ligand that acts in minutes and is not affected by blocking NF-κB. We also believe that previously described inhibitory effects of pertussis toxin on TNF-induced leakiness (Brett *et al.*, 1989) may be better explained by the elevation in cAMP produced by pertussis toxin than by any direct effect on TNF signaling.

Previous reports have shown that adenoviral transduction of EC with SR-IκB render EC sensitive to TNF-mediated apoptosis (Ferran *et al.*, 1998; Deshpande *et al.*, 2000). We did not observe this in our experiments. TNF-treated SRIκB-HDMEC were fully resistant to substrate-detachment as assessed by phase microscopy, to nuclear condensation, and fragmentation by fluorescence microscopy of 4′,6-diamidino-2-phenylindole, dihydrochloride staining, and to loss of membrane integrity by propidium iodide dye exclusion (unpublished observations, PRC and MSK). A possible explanation for their escape from apoptosis is that blockade of NF-κB activation was incomplete, either owing to a lower level of SR-IκB achieved with retroviral transduction than with adenovirus transduction or plasmid transfection, or owing to use of a mouse rather than a human SRIκB construct. Indeed, we did not see total inhibition of ICAM-1 expression (Figure S2), nor did we see a complete loss of cellular FADD-like IL-1β-converting enzyme-inhibitory protein (c-FLIP) expression (unpublished observations, MSK and PRC), a key NF-κB-dependent antiapoptotic protein. It has been reported that post-confluent HUVEC expressing SRIκB can resist apoptosis after TNF treatment (Cota-Gomez *et al.*, 2002) and that VEGF can promote EC survival under confluent conditions (Spyridopoulos *et al.*, 1997; Carmeliet *et al.*, 1999; Grazia Lampugnani *et al.*, 2003). Thus, either VEGF present in the growth medium or our use of post-confluent HDMEC may have counter-balanced the TNF signal for apoptosis as well. Whatever the explanation, our data suggest targeting endothelial NF-κB is a potential anti-inflammatory therapy so long as blockade is incomplete.

A final point of discussion is that our *in vitro* experiments do not take into account the possible contributions of leukocytes to vascular leak. We noted that ICAM-1 knockout mice show less leakiness at sites of inflammation in contact sensitivity responses (Sligh *et al.*, 1993; Xu *et al.*, 1994). This may well result from the absence of ICAM-1-stimulated leukocyte activation rather than (or in addition to) its role within EC. Indeed, many of the previous studies linking NF-κB to vascular leak are better explained as effects on protein (e.g., cytokine) synthesis by leukocytes rather than on EC effects (Moine *et al.*, 2000; Gautam *et al.*, 2001; Lentsch and Ward, 2001). However, these studies do not rule out a role for activation of NF-κB in EC. For example, exogenous administration of secretory leukocyte protease inhibitor, a naturally occurring NF-κB inhibitor expressed by EC, inhibits vascular leak *in vivo* and attenuates pulmonary vascular expression of ICAM-1 without affecting macrophage NF-κB (Lentsch *et al.*, 1999; Lentsch and Ward, 2001). Moreover, leak can occur without leukocytes present, for example in settings of neutropenia (Ognibene *et al.*, 1986). More pertinent to this study, leukocyte ligand engagement may induce ICAM-1 oligomerization, contributing to ICAM-1-mediated signaling by clustering endothelial ICAM-1 molecules (Wojciak-Stothard *et al.*, 1999; Barreiro *et al.*, 2002). However, it is possible that at sufficiently high levels of expression, ICAM-1 may spontaneously oligomerize on EC and signal without leukocyte engagement (Yang *et al.*, 2004) and like TNF receptors that are normally activated by ligand-induced clustering (Gaeta *et al.*, 2000), may spontaneously signal when simply overexpressed in EC. Leukocyte-independent clustering may potentially explain why the responses we observed with ICAM-1 transduction *in vitro* without leukocytes present required higher concentrations of ICAM-1 than are necessary *in vivo*, and if clustering does underlie the fall in TEER at high levels of ICAM-1 expression, then it would be expected to occur in $ICAM^{\Delta Cyto}$, which retains both of the extracellular domains believed to promote dimerization (Yang *et al.*, 2004).

In conclusion, we have presented evidence that increased ICAM-1 expression on HDMEC can mediate vascular leak and cell shape change, a putative means of coordinating leakiness with leukocyte recruitment. However, our data also suggest that while increased ICAM-1 expression may underlie some of the EC effects of TNF, it is unlikely to be the only TNF-induced protein that contributes to such changes.

MATERIALS AND METHODS

Reagents

TNF was obtained from R&D Systems (TNFα, Minneapolis, MN) and recombinant bovine thrombin from Amersham Biosciences Corp

(Piscataway, NJ). Unless specified, all other reagents were from Sigma-Aldrich Corp. (St Louis, MO).

HDMEC cultures

All human materials were obtained with patient consent and in compliance with the Declaration of Helsinki Principles under protocols approved by the Yale Human Investigations Committee. HDMEC were liberated from the superficial vascular plexus of the upper dermal layers of normal adult human skin obtained from discarded surgical specimens by dermatome, followed by digestion with Dispase (50 U/ml; BD Biosciences, San Jose, CA) for 30 minutes at 37°C and fine mincing as described previously (Kluger *et al.*, 1997). Released cells were cultured on 10 μg/ml human plasma fibronectin-coated plastic (Falcon, Lincoln Park, NJ) in EGM2-MV growth medium (Cambrex; East Rutherford, NJ). After 5–7 days in primary culture substrate-adherent cells were resuspended using trypsin and immunoselected on a mini-magnetic-activated cell sorter column using anti-CD-31-biotin followed by streptavidin-magnetic beads (Miltenyi Biotec, Auburn, CA). Immunoselected HDMEC were serially passaged on 0.1% gelatin-coated plastic and >99% free of contaminating leukocytes as assessed by immunohistochemistry and FACS analysis. In response to TNF, HDMEC uniformly upregulate ICAM-1 and VCAM-1 and express E-sel. The majority of the cells concomitantly express both venular (E-sel/CD62E, CD34) and lymphatic (podoplanin, Prox-1) markers. Confluent HDMEC monolayers develop well-formed inter-EC contacts that stain with mouse anti-human PECAM-1 (CD31) antibody (DAKO, Carpinteria, CA) adherens junctions that stain with goat anti-human VE-cadherin (CD144) antibody (Santa Cruz Biotechnology, Santa Cruz, CA), and tight junctions that stain with mouse anti-human ZO-1 (Zymed Laboratories, Inc., San Francisco, CA), features of blood vascular EC. As a result, HDMEC monolayers attain higher levels of TEER than HUVEC, which unlike cultured blood microvascular EC, lack tight junctions (Blum *et al.*, 1997). HDMEC were used between passage four through eight for the experiments described.

Retroviral transduction of HDMEC

Inserts for the translated region of human adhesion molecules ICAM-1 (gift of D. Altieri, University of Massachusetts Medical School, Worcester, MA) and human E-sel (Kluger *et al.*, 2002) were ligated between the long terminal repeat regions of the retroviral vector pLZRS immediately downstream of an inserted cytomegalovirus promoter (used in $ICAM^{med}$ and E-sel HDMEC), or into the same vector without the cytomegalovirus promoter (used to generate $ICAM^{high}$ HDMEC). A truncated ICAM-1 insert, missing a cytoplasmic domain except for the first, most membrane proximal Arg residue ($ICAM^{\Delta Cyto}$) was obtained by PCR and ligated into pLZRS. Identities of all constructs were confirmed by sequencing (a nucleotide mismatch was detected in the transmembrane domain of $ICAM^{\Delta Cyto}$ resulting in a conservative Leu502Val substitution) and immunoblotting. The pLZRS vector containing a cytomegalovirus promoter but minus any insert served as a negative control to transduce HDMEC. In NF-κB inhibition experiments, either the cDNA for the mouse S32/36A mutant IκBα super repressor of NF-κB (SRIκBα; gift of W. Min, Yale University School of Medicine) or enhanced green fluorescent protein control cDNA (Clontech Laboratories, Inc., Mountain View, CA) was inserted between the long terminal repeat regions of the pBMN.neo retroviral vector (gift of A. Bothwell, Yale University School of Medicine). A second HDMEC line transduced with the SRIκBα super repressor inserted into pLZRS with a cytomegalovirus promoter was compared to negative control consisting of vector without any insert. Retroviral supernatants produced by transfecting and selecting Phoenix packaging cells, were used for transducing HDMEC without selection (Kluger *et al.*, 2002) or (for the pBMN constructs only) with 1 mg/ml G418 selection (Invitrogen, Carlsbad, CA).

FACS analysis

Expression of ICAM-1 and E-sel on cultured HDMEC resuspended by trypsinization were determined by FACS analysis (FACSort, BD Biosciences) using CellQuestPro after immunostaining with saturating concentrations of mAbs, either anti-ICAM-1(CD54-FITC, Beckman-Coulter Inc., Fullerton, CA), anti-E-sel (CD62E-FITC; R&D Systems) or with isotype-matched FITC-labeled control antibodies. Adhesion molecule expression on HDMEC transduced with pBMN.neo retroviral vectors was determined by two-step immunostaining with mouse monoclonal primary antibodies R6.5 (anti-ICAM-1, gift of Boehringer-Ingelheim Pharmaceuticals Inc.), H 4/18 (anti-E-sel; Pober *et al.*, 1986a) or isotype-matched control antibodies followed by phycoerythrin-conjugated $F(ab')_2$ donkey anti-mouse secondary antibody (Jackson Labs, West Grove, PA) and FACS analysis with compensation for enhanced green fluorescent protein-generated fluorescence when needed. FACSorting was performed on a Becton Dickinson FACS Aria equipped with Becton Dickinson FACS Diva Version 4.1.2.

Measurement of TEER and transmonolayer flux of BSA

HDMEC were plated at 50% confluence onto 0.3 cm^2 human plasma fibronectin-coated (10 μg/ml) transwell inserts (BD Biosciences) and fed every 48 hours until formed into a tight monolayer. At 5 or more days, corresponding to 48–96 hours post-visual confluence, TEER measurements made daily with a transepithelial voltohmmeter (World Precision Instruments, Sarasota, FL) stabilized at 110–150 Ω. Four to six replicate wells were measured per treatment condition. All TEER values reported were corrected by subtracting the resistance of a naked transwell (typically 50 Ω). HDMEC were cultured to $\geqslant$48 hours post-confluence before addition of cytokine to upper and lower transwell chambers in experiments involving cytokine. The TNF-induced change in TEER expressed as a percentage of TEER measurements taken at identical time points on replicate cultures of vehicle-treated control HDMEC was computed as: $((TEER^{TNF}/TEER^{Vehicle} \times 100)-100)$. Flux of FITC-BSA (1 mg/ml) across HDMEC monolayers that had reached peak levels of TEER was measured by quantifying the fluorescence (excitation 485 nm, emission 530 nm) of medium collected from individual transwell bottom chambers with a CytoFluor II fluorescence plate reader (PerSeptive Biosystems, Framingham, MA). Values measured were corrected for background by subtracting the fluorescence of fresh medium and interpolated relative to a standard curve derived from graduated FITC-BSA concentrations.

Microscopy and morphometry

Confluent HDMEC monolayers on gelatin-coated cell culture plastic were washed twice in phosphate-buffered saline (PBS) containing

Ca^{++} and Mg^{++}, fixed in 4% paraformaldehyde/PBS 30 minutes at room temperature (for cell shape measurements) and blocked overnight in 0.1% saponin, 5% donkey serum, 1% BSA in PBS at 4°C. For morphometric determination of HDMEC shape, cell borders were labeled by immunostaining with goat anti-human VE cadherin (sc-6458; Santa Cruz Biotechnology) overnight at 4°C followed by donkey anti-goat Alexafluor 594 or 488 with 4′,6-diamidino-2-phenylindole, dihydrochloride (Molecular Probes, Carlsbad, CA) for 1 hour at room temperature. The same procedure, but with phalloidin-594 (also Molecular Probes) diluted 1:60 in buffer was followed for visualization of the actin cytoskeleton in HDMEC grown on human plasma fibronectin-coated glass cover slips. Fluorescence images, digitally captured with a Zeiss Axiovert 200M microscope networked to a Macintosh G4 computer using OpenLab software, version 4.0.3, were morphometrically analyzed by ImageJ 1.32 software (http://rsb.info.nih.gov/ij/). Cell shape, specifically the degree of elongation relative to a perfect circle, was measured in a blinded manner as an axis ratio (also termed ''aspect ratio''), defined as the ratio of the maximally long cell axis to a bisecting, perpendicular axis, as performed by others (Yu *et al.*, 1997; Wojciak-Stothard and Ridley, 2003). The patterns of ZO-1 and VE-cadherin distribution on HDMEC monolayers fixed in 95% ethanol/5% acetic acid and immunostained as described above were measured on 6–16 high power (× 63 objective) fields per transductant using ImageJ 1.32 (Macconi *et al.*, 2006).

Quantification of F- and G-actin by immunoblot analysis

Confluent monolayers of wild-type (treated ± TNF for 24 hours) or transduced HDMEC lines were washed at room temperature with 1 × PBS containing 1 μg/ml phalloidin (Sigma) to prevent filament disassembly, and soluble G-actin was extracted from the cells with actin extraction buffer I (1 × PBS/1% Triton X-100/2 μg/ml phalloidin) for 2 minutes as described (Cramer *et al.*, 2002). Lysates were collected and the monolayers were washed three more times. Insoluble F-actin was extracted with Actin Extraction Buffer II (1 × PBS/1% Triton X-100/2% SDS). Extracted protein lysates were resolved by SDS-PAGE and proteins were transferred to Immobilon-P polyvinylidene fluoride (Millipore, Bedford, MA). After blocking in 5% non-fat milk (Bio-Rad, Hercules, CA), β-actin was detected on the membrane using mouse anti-human β-actin mAb (Sigma: Clone AC-74). Band intensity was quantified using a Molecular Dynamics Densitometer and MD ImageQuant v3.31 software.

SiRNA knockdown

HDMEC were plated on to gelatin-coated 12-well plates at approximately 50% confluence. Mixtures of Oligofectamine to 20 μl/ml and siRNA to 50 nM were prepared in Opti-MEM I Reduced Serum Medium (all from Invitrogen). At 24 hours post-plating, concentrated mixtures of siRNA complexes (Dharmacon Inc., Chicago, IL) were diluted 5-fold to a siRNA concentration of 10 nM before co-incubation with HDMEC cultures for 6 hours at 37°C. Fresh medium was added overnight and cells were re-transfected 24 hours later, rested for 24 hours, and then treated with 10 ng/ml human TNF for 24 hours before morphometric analysis or immunostaining followed by FACS analysis. The four siRNA used to specifically target ICAM-1 (Vickers *et al.*, 2003) did not inhibit TNF-induced expression of E-sel (data not shown).

Statistical analysis

Significance of differences among two groups was tested by an unpaired *t*-test and among more than two groups, by one-way analysis of variance (ANOVA) followed by the Dunnet's post-test in single variable experiments, or by two-way ANOVA followed by the Bonferroni post-test in two variable experiments. *P*-values <0.05 were accepted as significant. All results were computed using Prism version 4.0c and are presented as means ± SEM. A sigmoid curve nonlinear fit analysis was used to describe the concentration dependence of TNF-induced changes in ICAM-1 expression, leakiness, and shape measured on replicate cultures.

CONFLICT OF INTEREST

J.S.P serves as a consultant for Isis Pharmaceuticals Inc.

ACKNOWLEDGMENTS

We thank Lisa Gras for preparing HDMEC cultures, Drs Frank Giordano and William Sessa for sharing use of equipment and Dr Brenda Baker for providing and discussing use of siRNA reagents. Grant Support was provided from the NIH (RO1-HL 36003 and P30-AR041942-11). This project has also been funded in part with Federal funds from the National Heart, Lung, and Blood Institute, National Institutes of Health, under contract No. N01-HV-28186.

SUPPLEMENTARY MATERIAL

Figure S1. FACS analysis of $ICAM^{\Delta Cyto}$ expression on HDMEC.

Figure S2. ICAM-1 surface expression on SRIκB- and enhanced green fluorescent protein-transduced HDMEC after TNF (10 ng/ml for 24 hours).

Table S1. SiRNA reagents used.

REFERENCES

Adamson P, Etienne S, Couraud PO, Calder V, Greenwood J (1999) Lymphocyte migration through brain endothelial cell monolayers involves signaling through endothelial ICAM-1 via a rho-dependent pathway. *J Immunol* 162:2964–73

Amos C, Romero IA, Schultze C, Rousell J, Pearson JD, Greenwood J *et al.* (2001) Cross-linking of brain endothelial intercellular adhesion molecule (ICAM)-1 induces association of ICAM-1 with detergent-insoluble cytoskeletal fraction. *Arterioscler Thromb Vasc Biol* 21: 810–6

Barreiro O, Yanez-Mo M, Serrador JM, Montoya MC, Vicente-Manzanares M, Tejedor R *et al.* (2002) Dynamic interaction of VCAM-1 and ICAM-1 with moesin and ezrin in a novel endothelial docking structure for adherent leukocytes. *J Cell Biol* 157:1233–45

Bazzoni G, Dejana E (2004) Endothelial cell-to-cell junctions: molecular organization and role in vascular homeostasis. *Physiol Rev* 84:869–901

Blum MS, Toninelli E, Anderson JM, Balda MS, Zhou J, O'Donnell L *et al.* (1997) Cytoskeletal rearrangement mediates human microvascular endothelial tight junction modulation by cytokines. *Am J Physiol* 273:H286–94

Brett J, Gerlach H, Nawroth P, Steinberg S, Godman G, Stern D (1989) Tumor necrosis factor/cachectin increases permeability of endothelial cell monolayers by a mechanism involving regulatory G proteins. *J Exp Med* 169:1977–91

Carmeliet P, Lampugnani MG, Moons L, Breviario F, Compernolle V, Bono F *et al.* (1999) Targeted deficiency or cytosolic truncation of the VE-cadherin gene in mice impairs VEGF-mediated endothelial survival and angiogenesis. *Cell* 98:147–57

Carpen O, Pallai P, Staunton DE, Springer TA (1992) Association of intercellular adhesion molecule-1 (ICAM-1) with actin-containing cytoskeleton and alpha-actinin. *J Cell Biol* 118:1223–34

Collins T, Read MA, Neish AS, Whitley MZ, Thanos D, Maniatis T (1995) Transcriptional regulation of endothelial cell adhesion molecules: NF-kappa B and cytokine-inducible enhancers. *FASEB J* 9:899–909

Corada M, Mariotti M, Thurston G, Smith K, Kunkel R, Brockhaus M *et al.* (1999) Vascular endothelial-cadherin is an important determinant of microvascular integrity *in vivo*. *Proc Natl Acad Sci USA* 96: 9815–20

Cota-Gomez A, Flores NC, Cruz C, Casullo A, Aw TY, Ichikawa H *et al.* (2002) The human immunodeficiency virus-1 Tat protein activates human umbilical vein endothelial cell E-selectin expression via an NF-kappa B-dependent mechanism. *J Biol Chem* 277: 14390–9

Cotran RS, Pober JS, Gimbrone MA Jr, Springer TA, Wiebke EA, Gaspari AA *et al.* (1988) Endothelial activation during interleukin 2 immunotherapy. A possible mechanism for the vascular leak syndrome. *J Immunol* 140:1883–8

Cramer LP, Briggs LJ, Dawe HR (2002) Use of fluorescently labelled deoxyribonuclease I to spatially measure G-actin levels in migrating and non-migrating cells. *Cell Motil Cytoskeleton* 51:27–38

Crowley SR (1996) The pathogenesis of septic shock. *Heart Lung* 25: 124–34

Deshpande SS, Angkeow P, Huang J, Ozaki M, Irani K (2000) Rac1 inhibits TNF-alpha-induced endothelial cell apoptosis: dual regulation by reactive oxygen species. *FASEB J* 14:1705–14

Detmar M, Imcke E, Ruszczak Z, Orfanos CE (1990) Effects of recombinant tumor necrosis factor-alpha on cultured microvascular endothelial cells derived from human dermis. *J Invest Dermatol* 95:219S–22S

Dubinett SM, Huang M, Lichtenstein A, McBride WH, Wang J, Markovitz G *et al.* (1994) Tumor necrosis factor-alpha plays a central role in interleukin-2-induced pulmonary vascular leak and lymphocyte accumulation. *Cell Immunol* 157:170–80

Ferran C, Stroka DM, Badrichani AZ, Cooper JT, Wrighton CJ, Soares M *et al.* (1998) A20 inhibits NF-kappaB activation in endothelial cells without sensitizing to tumor necrosis factor-mediated apoptosis. *Blood* 91:2249–58

Gaeta ML, Johnson DR, Kluger MS, Pober JS (2000) The death domain of tumor necrosis factor receptor 1 is necessary but not sufficient for Golgi retention of the receptor and mediates receptor desensitization. *Lab Invest* 80:1185–94

Gautam N, Olofsson AM, Herwald H, Iversen LF, Lundgren-Akerlund E, Hedqvist P *et al.* (2001) Heparin-binding protein (HBP/CAP37): a missing link in neutrophil-evoked alteration of vascular permeability. *Nat Med* 7:1123–7

Grazia Lampugnani M, Zanetti A, Corada M, Takahashi T, Balconi G, Breviario F *et al.* (2003) Contact inhibition of VEGF-induced proliferation requires vascular endothelial cadherin, beta-catenin, and the phosphatase DEP-1/CD148. *J Cell Biol* 161:793–804

Groeneveld AB (2002) Vascular pharmacology of acute lung injury and acute respiratory distress syndrome. *Vascul Pharmacol* 39:247–56

Heiska L, Alfthan K, Gronholm M, Vilja P, Vaheri A, Carpen O (1998) Association of ezrin with intercellular adhesion molecule-1 and -2 (ICAM-1 and ICAM-2). Regulation by phosphatidylinositol 4, 5-bisphosphate. *J Biol Chem* 273:21893–900

Kluger MS (2004) Vascular endothelial cell adhesion and signaling during leukocyte recruitment. *Adv Dermatol* 20:163–201

Kluger MS, Johnson DR, Pober JS (1997) Mechanism of sustained E-selectin expression in cultured human dermal microvascular endothelial cells. *J Immunol* 158:887–96

Kluger MS, Shiao SL, Bothwell ALM, Pober JS (2002) Cutting edge: internalization of transduced E-selectin by cultured human endothelial cells: comparison of dermal microvascular and umbilical vein cells and identification of a phosphoserine-type di-leucine motif. *J Immunol* 168:2091–5

Koss M, Pfeiffer GR II, Wang Y, Thomas ST, Yerukhimovich M, Gaarde WA *et al.* (2006) Ezrin/radixin/moesin proteins are phosphorylated by TNF-alpha and modulate permeability increases in human pulmonary microvascular endothelial cells. *J Immunol* 176:1218–27

Lentsch AB, Jordan JA, Czermak BJ, Diehl KM, Younkin EM, Sarma V *et al.* (1999) Inhibition of NF-kappaB activation and augmentation of IkappaBbeta by secretory leukocyte protease inhibitor during lung inflammation. *Am J Pathol* 154:239–47

Lentsch AB, Ward PA (2001) Regulation of experimental lung inflammation. *Respir Physiol* 128:17–22

Lo SK, Everitt J, Gu J, Malik AB (1992) Tumor necrosis factor mediates experimental pulmonary edema by ICAM-1 and CD18-dependent mechanisms. *J Clin Invest* 89:981–8

Macconi D, Abbate M, Morigi M, Angioletti S, Mister M, Buelli S *et al.* (2006) Permselective dysfunction of podocyte-podocyte contact upon angiotensin II unravels the molecular target for renoprotective intervention. *Am J Pathol* 168:1073–85

Majno G, Palade GE (1961) Studies on inflammation. 1. The effect of histamine and serotonin on vascular permeability: an electron microscopic study. *J Biophys Biochem Cytol* 11:571–605

Majno G, Shea SM, Leventhal M (1969) Endothelial contraction induced by histamine-type mediators: an electron microscopic study. *J Cell Biol* 42:647–72

Marcus BC, Gewertz BL (1998) Measurement of endothelial permeability. *Ann Vasc Surg* 12:384–90

McDonald DM, Thurston G, Baluk P (1999) Endothelial gaps as sites for plasma leakage in inflammation. *Microcirculation* 6:7–22

Moine P, McIntyre R, Schwartz MD, Kaneko D, Shenkar R, Le Tulzo Y *et al.* (2000) NF-kappaB regulatory mechanisms in alveolar macrophages from patients with acute respiratory distress syndrome. *Shock* 13:85–91

Munro JM, Pober JS, Cotran RS (1989) Tumor necrosis factor and interferon-gamma induce distinct patterns of endothelial activation and associated leukocyte accumulation in skin of Papio anubis. *Am J Pathol* 135: 121–33

Nwariaku FE, Rothenbach P, Liu Z, Zhu X, Turnage RH, Terada LS (2003) Rho inhibition decreases TNF-induced endothelial MAPK activation and monolayer permeability. *J Appl Physiol* 95:1889–95

Ognibene FP, Martin SE, Parker MM, Schlesinger T, Roach P, Burch C *et al.* (1986) Adult respiratory distress syndrome in patients with severe neutropenia. *N Engl J Med* 315:547–51

Pober JS, Bevilacqua MP, Mendrick DL, Lapierre LA, Fiers W, Gimbrone MA Jr (1986a) Two distinct monokines, interleukin 1 and tumor necrosis factor, each independently induce biosynthesis and transient expression of the same antigen on the surface of cultured human vascular endothelial cells. *J Immunol* 136:1680–7

Pober JS, Cotran RS (1991) Immunologic interactions of T lymphocytes with vascular endothelium. *Adv Immunol* 50:261–302

Pober JS, Gimbrone MA Jr, Lapierre LA, Mendrick DL, Fiers W, Rothlein R *et al.* (1986b) Overlapping patterns of activation of human endothelial cells by interleukin 1, tumor necrosis factor, and immune interferon. *J Immunol* 137:1893–6

Richard L, Velasco P, Detmar M (1998) A simple immunomagnetic protocol for the selective isolation and long-term culture of human dermal microvascular endothelial cells. *Exp Cell Res* 240:1–6

Sligh J Jr, Ballantyne C, Rich S, Hawkins H, Smith C, Bradley A *et al.* (1993) Inflammatory and immune responses are impaired in mice deficient in intercellular adhesion molecule 1. *Proc Natl Acad Sci USA* 90: 8529–33

Spyridopoulos I, Brogi E, Kearney M, Sullivan AB, Cetrulo C, Isner JM *et al.* (1997) Vascular endothelial growth factor inhibits endothelial cell apoptosis induced by tumor necrosis factor-alpha: balance between growth and death signals. *J Mol Cell Cardiol* 29:1321–30

Stevens T, Garcia JG, Shasby DM, Bhattacharya J, Malik AB (2000) Mechanisms regulating endothelial cell barrier function. *Am J Physiol Lung Cell Mol Physiol* 279:L419–22

Stolpen AH, Guinan EC, Fiers W, Pober JS (1986) Recombinant tumor necrosis factor and immune interferon act singly and in combination to reorganize human vascular endothelial cell monolayers. *Am J Pathol* 123:16–24

Thom AK, Alexander HR, Andrich MP, Barker WC, Rosenberg SA, Fraker DL (1995) Cytokine levels and systemic toxicity in patients undergoing isolated limb perfusion with high-dose tumor necrosis factor, interferon gamma, and melphalan. *J Clin Oncol* 13:264–73

Vickers TA, Koo S, Bennett CF, Crooke ST, Dean NM, Baker BF (2003) Efficient reduction of target RNAs by small interfering RNA and RNase

H-dependent antisense agents. A COMPARATIVE ANALYSIS. *J Biol Chem* 278:7108–18

von Andrian UH, Mackay CR (2000) T-cell function and migration – two sides of the same coin. *N Engl J Med* 343:1020–34

Wang Q, Pfeiffer GR II, Stevens T, Doerschuk CM (2002) Lung microvascular and arterial endothelial cells differ in their responses to intercellular adhesion molecule-1 ligation. *Am J Respir Crit Care Med* 166:872–7

Wojciak-Stothard B, Entwistle A, Garg R, Ridley AJ (1998) Regulation of TNF-alpha-induced reorganization of the actin cytoskeleton and cell-cell junctions by Rho, Rac, and Cdc42 in human endothelial cells. *J Cell Physiol* 176:150–65

Wojciak-Stothard B, Ridley AJ (2003) Shear stress-induced endothelial cell polarization is mediated by Rho and Rac but not Cdc42 or PI 3-kinases. *J Cell Biol* 161:429–39

Wojciak-Stothard B, Williams L, Ridley AJ (1999) Monocyte adhesion and spreading on human endothelial cells is dependent on Rho-regulated receptor clustering. *J Cell Biol* 145:1293–307

Wysolmerski RB, Lagunoff D (1990) Involvement of myosin light-chain kinase in endothelial cell retraction. *Proc Natl Acad Sci USA* 87:16–20

Xu H, Gonzalo JA, St Pierre Y, Williams IR, Kupper TS, Cotran RS *et al.* (1994) Leukocytosis and resistance to septic shock in intercellular adhesion molecule 1-deficient mice. *J Exp Med* 180:95–109

Yang Y, Jun CD, Liu JH, Zhang R, Joachimiak A, Springer TA *et al.* (2004) Structural basis for dimerization of ICAM-1 on the cell surface. *Mol Cell* 14:269–76

Yu PK, Yu D, Alder VA, Seydel U, Su E, Cringle SJ (1997) Heterogeneous endothelial cell structure along the porcine retinal microvasculature. *Exp Eye Res* 65:379–89